

# 1.55- $\mu\text{m}$ InP–InGaAsP Fabry–Pérot Lasers With Integrated Spot Size Converters Using Antiresonant Reflecting Optical Waveguides

Marko Galarza, Kurt De Mesel, Steven Verstuyft, Cándido Aramburu, Ingrid Moerman, *Member, IEEE*, Peter Van Daele, *Member, IEEE*, Roel Baets, *Senior Member, IEEE*, and Manuel López-Amo, *Senior Member, IEEE*

**Abstract**—We demonstrate a new concept for InGaAsP–InP 1.55- $\mu\text{m}$  Fabry–Pérot lasers integrated with spot size converters using type-A antiresonant reflecting optical waveguides. The fabrication of such devices allows to avoid the growth of thick layers of quaternary material with low Ga and As fraction, which are difficult to achieve and grow. Reduced far-field divergence angles ( $10^\circ \times 27^\circ$ ) and improved coupling to cleaved standard single-mode fibers (2.6-dB coupling loss) are achieved. The proposed device is compatible with conventional epitaxial techniques and lithographic methods.

**Index Terms**—Optical couplers, optical waveguides, semiconductor device modeling, semiconductor device packaging, semiconductor lasers.

## I. INTRODUCTION

THE MAJOR part of the cost of an optical module comes from the packaging. This fact is one of the largest barriers to future mass production needs in optical communication systems. Highly efficient chip-to-fiber coupling with large alignment tolerances is very important for low-loss integrated optics. The problem arises from the large mismatch between the large circular mode in the fiber and the small asymmetric mode in a III–V semiconductor waveguide component, leading to high coupling losses. Over the past years, much research has focused on the integration of mode size converters with waveguide components in order to improve the coupling efficiency [1], [2]. Most of these approaches involve complex growth and/or processing steps, requiring extensive process development [3]. Nevertheless, there is a group of devices requiring only a single standard planar epitaxial growth step and conventional processing techniques that has attracted considerable attention [4]–[6]. These devices incorporate a large fiber-adapted rib waveguide that operates close to cutoff. In InP technology, this involves the growth of quaternary materials exhibiting a slightly higher refractive index than the InP substrate. These low refractive indexes are achieved by means

Manuscript received January 9, 2002; revised April 12, 2002. This work was supported in part by Spanish CICYT under Project TIC2001–0877-C02–02 and by Gobierno de Navarra from a grant.

M. Galarza, C. Aramburu, and M. López-Amo are with the Electric and Electronic Department, Public University of Navarre, Campus de Arrosadía, 31006 Pamplona, Navarra, Spain.

K. De Mesel, S. Verstuyft, I. Moerman, P. Van Daele, and R. Baets are with the Department of Information Technology, Ghent University-IMEC, B-9000 Ghent, Belgium (e-mail: mgalarza@intec.rug.ac.be).

Publisher Item Identifier S 1041-1135(02)06087-1.

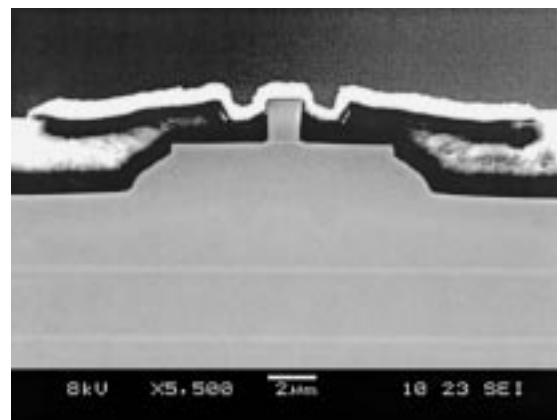
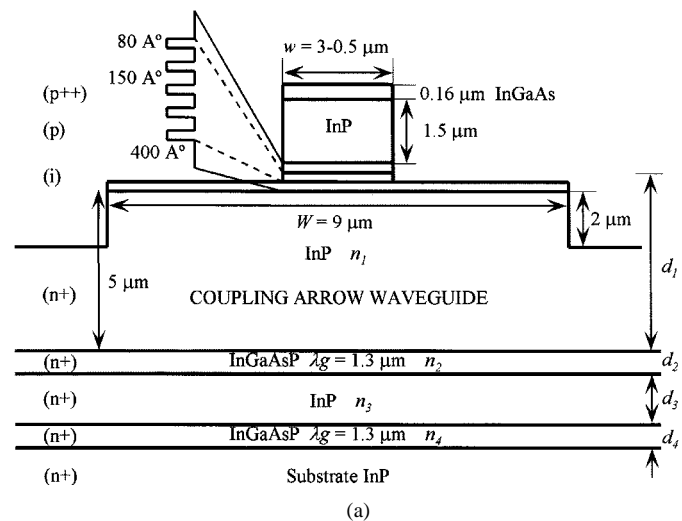


Fig. 1. Cross section of the mode expanded laser. (a) Schematic drawing. (b) SEM photograph.

of low Ga- and As-fraction quaternary materials, which are difficult to achieve and grow. One solution is the use of diluted structures. The new taper concept presented in this work is based on the use of type-A ARROW waveguides [7] and forms an alternative solution to this problem. The design, fabrication, and performance of the new device are discussed.

## II. DEVICE DESIGN AND FABRICATION

The transverse structure of the proposed laser is shown in Fig. 1. The device is grown by metal–organic chemical vapor deposition (MOCVD) and consists of an active waveguide, which

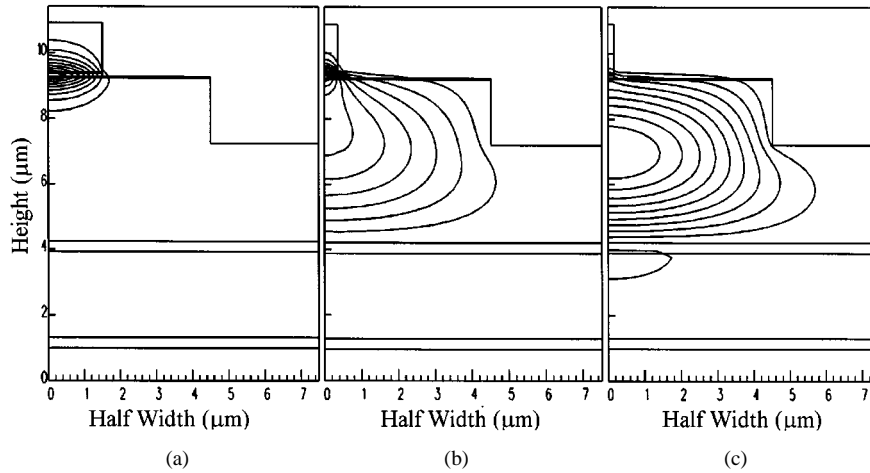


Fig. 2. The fundamental TE mode for (a)  $w = 3 \mu\text{m}$ , (b)  $w = 0.9 \mu\text{m}$ , and (c)  $w = 0.5 \mu\text{m}$ .

is placed on top of a large passive ridge that is optimized for coupling to an optical fiber. The vertical optical confinement in this passive guide is realized by a type-A ARROW structure. The quasiguided ARROW-modes exhibit very attractive features for a fiber coupling function: large mode sizes, low losses for the fundamental mode, high discrimination of the higher order modes, and ease of fabrication owing to its high tolerances and to the fact that the thick core consists of InP. Moreover, the wavelength and polarization dependence of such waveguides is negligible. The optimum thickness of the three ARROW cladding layers ( $d_2$ ,  $d_3$ ,  $d_4$ ) is given by the following approximate antiresonance conditions [8]:

$$d_{2,4} = \frac{\lambda}{4n_{2,4}} \left( 1 - \left( \frac{n_1}{n_{2,4}} \right)^2 + \left( \frac{\lambda}{2n_{2,4}d_{ce}} \right)^2 \right)^{-1/2} \cdot (2M + 1)$$

$$d_3 = \frac{d_{ce}}{2} (2N + 1) \quad (M, N = 0, 1, 2, \dots) \quad (1)$$

where  $\lambda$  is the vacuum wavelength;  $n_1$ ,  $n_2$ ,  $n_4$  the refractive index of the ARROW InP core, the first cladding layer and the third, respectively;  $d_{ce}$  is the equivalent core thickness, which involves the Goos-Hänchen shift at the top of the ARROW core and is defined as

$$d_{ce} = d_1 + \zeta \frac{\lambda}{2\pi \sqrt{n_{co}^2 - n_0^2}} \quad (2)$$

where

$$\zeta = \begin{cases} 1, & \text{for TE modes} \\ (n_0/n_{co})^2, & \text{for TM modes.} \end{cases} \quad (3)$$

In the above expressions,  $n_{co}$  denotes the refractive index of the active core, and  $n_0$  denotes the refractive index of the polyimide that covers the device. We choose a quaternary compound with  $\lambda_g = 1.3 \mu\text{m}$  for the two high-refractive index ARROW layers. The calculated values of the cladding layer thickness for TE polarization are:  $d_{2,4} = 0.32 \mu\text{m}$  and  $d_3 = 2.6 \mu\text{m}$ .

The multiple quantum-well (MQW) contains five 1% compressively strained 80-Å-thick  $\text{In}_{0.78}\text{Ga}_{0.22}\text{As}_{0.79}\text{P}_{0.21}$  wells for emission at  $1.55 \mu\text{m}$ , and four lattice-matched 150-Å-thick  $\text{In}_{0.75}\text{Ga}_{0.25}\text{As}_{0.54}\text{P}_{0.46}$  barriers, surrounded by 400-Å-thick

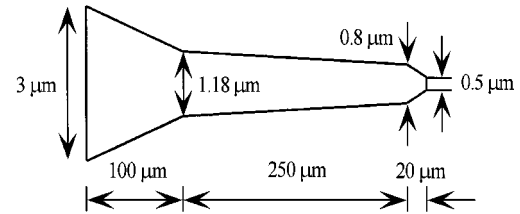


Fig. 3. The optimum taper shape is approximated by a piecewise linear device consisting of three linear sections.

undoped confining layers having the same composition of the barriers. The metallization covers the spot size converters over their entire length. This can have a negative impact on the threshold current and efficiency, but on the other hand it avoids the risk of high absorption losses in the passive section of the taper.

As the active waveguide is tapered by reducing the ridge width from 3 to  $0.5 \mu\text{m}$ , the mode couples adiabatically from the upper guide to the underlying ARROW waveguide (see Fig. 2). The design of the lateral tapering is based on the adiabaticity of the mode transformation, and has been evaluated by means of a commercial three-dimensional (3-D) eigenmode expansion algorithm based on a resonance method [9]. The critical change of the modal shape and the whole radiation is produced in the 1.18- to  $0.8 \mu\text{m}$  range, where low taper angles will be needed to obtain an adiabatic mode transformation. The taper shape was approximated by a  $370\text{-}\mu\text{m}$ -long piecewise linear device consisting of three linear sections as shown in Fig. 3, and exhibits a calculated transformation loss of 1 dB.

### III. DEVICE RESULTS

The devices were operated in continuous-wave (CW) mode. Fig. 4 shows the light versus current ( $L-I$ ) characteristics of four expanded mode devices and a control sample without any tapers. Untapered  $750\text{-}\mu\text{m}$ -long and  $3\text{-}\mu\text{m}$ -wide reference lasers exhibit typical threshold currents  $I_{th}$  of 30 mA and an external efficiency of 0.13 W/A, while the expanded mode devices consisting of a  $500\text{-}\mu\text{m}$ -long gain section and a  $370\text{-}\mu\text{m}$ -long taper, show a threshold current around 50 mA with an external efficiency of 0.15 W/A. The increase in the threshold current of the

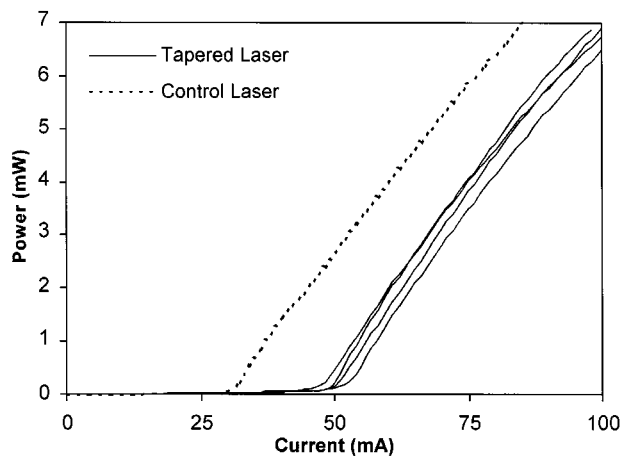


Fig. 4.  $L$ - $I$  characteristics of several mode expanded lasers compared to a control laser without any taper.

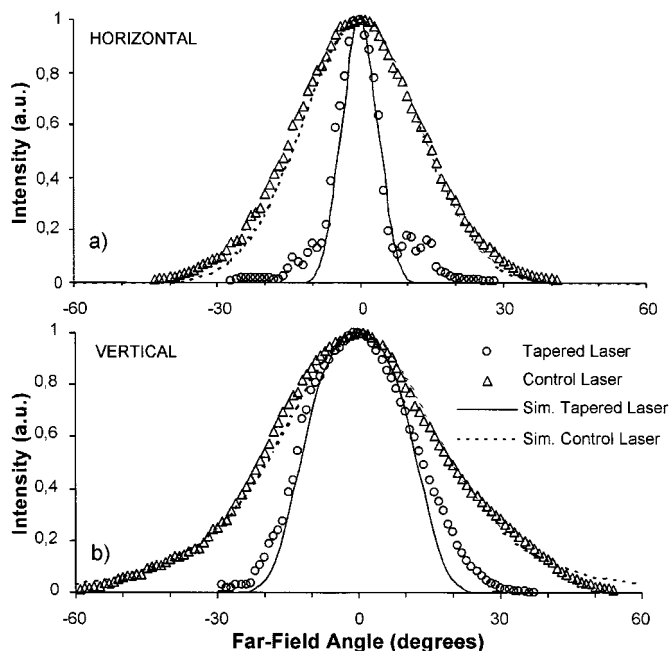


Fig. 5. Far-field emission patterns of tapered and untapered lasers. (a) Lateral direction. (b) Transverse direction.

expanded-mode lasers, as compared to the reference samples, can be attributed to the radiated power in the beam transformation region, to the losses in the n-doped thick InP layer, and to the nonuniform pumping of the tapered active rib as a function of its width. The decrease of the tapered facet reflectivity makes the external efficiency to increase slightly.

The far-field emission patterns for both the tapered laser and the control samples were measured by using a rotating stage and a pinhole detector (see Fig. 5). The theoretical curves obtained

from the Fourier transform of the theoretical near fields are also overlaid in Fig. 5, for comparison. A far-field divergence angle [full-width at half-maximum (FWHM)] of  $10^\circ \times 27^\circ$  was obtained in lateral and vertical directions for the mode expanded laser, while the untapered devices exhibited  $30.1^\circ \times 40.1^\circ$ , in good agreement with theoretical calculations.

A coupling efficiency measurement was performed between the expanded mode laser and a standard cleaved SMF with a spot size of  $10 \mu\text{m}$  at  $1.55 \mu\text{m}$ . A maximum coupling efficiency of 55% (2.6-dB loss) was obtained (this includes the Fresnel losses occurring at the air-glass interface). The improvement in the fiber coupling with respect to the untapered lasers reaches 5.8 dB. The measured 1-dB alignment tolerance range is  $4.4 \mu\text{m}$  in lateral direction and  $4.5 \mu\text{m}$  in transverse direction.

#### IV. CONCLUSION

We have realized a new laser emitting at  $1.55\text{-}\mu\text{m}$  wavelength integrated with a spot size converter using a type-A ARROW waveguide for enhanced fiber coupling. The confinement of the expanded field in the large InP core of the ARROW waveguide facilitates the fabrication because it allows to avoid the growth of low Ga- and As-fraction quaternary materials. Efficient mode transformation and considerable reduction of the horizontal and vertical far field have been achieved.

#### REFERENCES

- [1] J. E. Johnson *et al.*, "Monolithically integrated semiconductor optical amplifier and electroabsorption modulator with dual-waveguide spot-size converter input," *IEEE J. Select. Topics Quantum Electron.*, vol. 6, pp. 19–25, Jan. 2000.
- [2] J. R. Kim, J. S. Lee, S. Park, M. W. Park, J. S. Yu, S. D. Lee, A. G. Choo, T. I. Kim, and Y. H. Lee, "Spot-size converter integrated polarization insensitive semiconductor optical amplifiers," *IEEE Photon. Technol. Lett.*, vol. 11, pp. 967–969, Aug. 1999.
- [3] I. Moerman, P. Van Daele, and P. M. Demeester, "A review on fabrication technologies for the monolithic integration of tapers with III-V semiconductor devices," *IEEE J. Select. Topics Quantum Electron.*, vol. 3, pp. 1308–1320, Dec. 1997.
- [4] S. S. Saini, F. G. Johnson, D. R. Stone, H. Shen, W. Zhou, and M. Dagenais, "Passive active resonant coupler (PARC) platform with mode expander," *IEEE Photon. Technol. Lett.*, vol. 12, pp. 1025–1027, Aug. 2000.
- [5] G. A. Vawter, R. E. Smith, H. Hou, and J. R. Wendt, "Semiconductor laser with tapered-rib adiabatic-following fiber coupler for expanded output-mode diameter," *IEEE Photon. Technol. Lett.*, vol. 9, pp. 425–427, Apr. 1997.
- [6] K. De Mesel, R. Baets, C. Sys, S. Verstuyft, I. Moerman, and P. Van Daele, "First demonstration of 980 nm oxide confined laser with integrated spot size converter," *Electron. Lett.*, vol. 36, pp. 1028–1029, Jun. 2000.
- [7] R. A. Soref and K. J. Ritter, "Silicon antiresonant reflecting optical waveguides," *Opt. Lett.*, vol. 15, pp. 792–794, Jul. 1990.
- [8] J. M. Kubica, "Numerical analysis of InP/InGaAsP ARROW waveguides using transfer matrix approach," *J. Lightwave Technol.*, vol. 10, pp. 767–771, Jun. 1992.
- [9] A. S. Sudbo, "Numerically stable formulation of the transverse resonance method for mode-field calculations in dielectric waveguides," *IEEE Photon. Technol. Lett.*, vol. 5, pp. 342–344, Mar. 1993.